ELSEVIER

Contents lists available at ScienceDirect

Atmospheric Research

journal homepage: www.elsevier.com/locate/atmosres





The effects of boundary layer vertical turbulent diffusivity on the tropical cyclone intensity

Lei Ye^a, Yubin Li^{a,b,c,*}, Ping Zhu^{d,*}, Zhiqiu Gao^{a,e}

- ^a Collaborative Innovation Center on Forecast and Evaluation of Meteorological Disasters, Key Laboratory for Aerosol-Cloud-Precipitation of China Meteorological Administration, School of Atmospheric Physics, Nanjing University of Information Science and Technology, Nanjing 210044, China
- ^b Southern Marine Science and Engineering Guangdong Laboratory (Zhuhai), Zhuhai 519000, China
- ^c China Meteorological Administration Xiongʻan Atmospheric Boundary Layer Key Laboratory, Xiongʻan New Area 071800, China
- ^d Department of Earth and Environment, Florida International University, Miami, FL 33199, USA
- e State Key Laboratory of Atmospheric Boundary Layer Physics and Atmospheric Chemistry, Institute of Atmospheric Physics, Chinese Academy of Sciences, Beijing 100029, China

ARTICLE INFO

Keywords: Planetary boundary layer Yonsei University scheme Turbulent diffusivity Tropical cyclone intensity

Numerical simulation

ABSTRACT

The sensitivity of the simulated intensification of Typhoon Mangkhut (2018) to boundary layer turbulent diffusivity (K_m) is investigated through a series of numerical simulations using the modified K_m from the Yonsei-University (YSU) planetary boundary layer (PBL) scheme in the Weather Research and Forecasting (WRF) model. Two intensity metrics, namely grid-point and area-averaged metrics, were employed to evaluate the simulations. The results indicate that a smaller K_m tends to result in a smaller grid-point minimum central sea level pressure (MSLP), while producing a larger area-averaged MSLP and smaller area-averaged maximum 10 m wind speed (VMAX), which is consistent with a weaker radial inflow averaged over the area of a 500 km radius. Furthermore, the surface latent heat flux exhibits a nearly linear relationship with K_m throughout the simulation. Overall, a larger K_m tends to produce a greater diabatic heating rate, although this relationship is not as clear as that between K_m and latent heat flux due to the presence of spontaneous asymmetric convective eddy features. Moreover, since a larger K_m tends to result in a larger 10 m tangential wind, the size of a tropical cyclone (TC) defined by the radius at which 10 m tangential wind speed becomes 10 m s⁻¹ shows a positive linear relationship with K_m .

1. Introduction

Tropical cyclone (TC) is one of the most destructive natural disasters causing severe loss of life and property damage (Sun and Barros, 2014; Nystrom et al., 2020). Over the past decades, with the development of numerical weather prediction models, TC forecast has improved significantly (Ma et al., 2018; Sun et al., 2019). However, accurate prediction of TC intensification remains challenging (Wang and Wang, 2014; Fox and Judt, 2018; Chang et al., 2020).

In general, large-scale environmental conditions such as vertical wind shear, upper-tropospheric divergence, sea surface temperature, ocean heat content, and moisture supply are the key external factors of TC intensification (Kaplan et al., 2015). Under favorable large-scale environmental conditions, TCs intensify through internal interactions among microphysical, cumulus, and planetary boundary layer (PBL)

processes (Lee and Wu, 2018). The PBL turbulence plays a dual-role in TC energetics. The turbulent enthalpy fluxes from the underlying ocean are major energy source for the storms, but on the other hand, the dissipation of turbulence kinetic energy (TKE) by the turbulence-induced friction serves as a primary sink of TC energy. The ratio between these two processes strongly influences the storm intensification rate (Kepert, 2012; Emanuel, 2018; Ming and Zhang, 2018), making the PBL a crucial component in TC dynamics (Emanuel, 2018). The theories for TC intensification, including the conditional instability of the second kind (CISK, Charney and Eliassen, 1964), the cooperative-intensification mechanism (Ooyama, 1964, 1982), the wind-induced surface heat exchange (WISHE, Emanuel, 2003), and the 3D rotating convective updraft paradigm (Montgomery and Smith, 2014), all recognize the role of the PBL in the TC intensification. Numerical studies have also demonstrated that turbulent processes in PBL play an essential role in the

E-mail addresses: liyubin@nuist.edu.cn (Y. Li), zhup@fiu.edu (P. Zhu).

^{*} Corresponding authors.

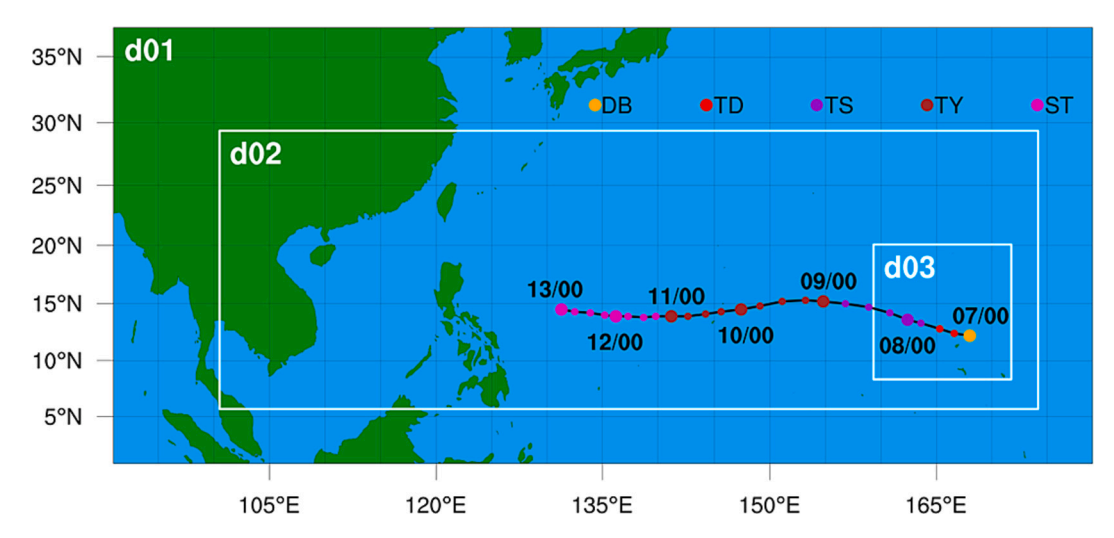


Fig. 1. Model domains and the best track of Mangkhut (2018) from Joint Typhoon Warning Center (JTWC) during the simulation period from 0000 UTC 7 to 0000 UTC 13 September 2018. Colored dots indicate the TC track and intensity (DB: disturbance; TD: tropical depression; TS: tropical storm; TY: typhoon; ST: super typhoon).

Table 1 The summary of modified K_m in YSU scheme from numerical experiments.

Experiment name	Turbulent diffusivity K_m
YSU	K_m
YSU_4Km	$4K_m$
YSU_2K _m	$2K_m$
$YSU_0.5K_m$	$0.5K_m$
$YSU_0.25K_m$	$0.25K_{m}$

intensification of TCs (e.g., Zhang and Rogers, 2019; Zhu et al., 2019; Zhu et al., 2021; Li and Wang, 2021a, 2021b).

Studies have shown that simulated TC intensity is very sensitive to the choice of PBL schemes. For instance, Li and Pu (2008) performed simulations using Weather Research and Forecasting (WRF) model and showed that the use of various PBL schemes resulted in differences in the simulated MSLP up to 19 hPa during the early rapid intensification of Hurricane Emily (2005). Kepert (2012) reviewed and assessed the performance of PBL schemes and suggested that the parameterization of vertical mixing in the PBL has a key impact on hurricane intensity and structure. Zhu et al. (2014) conducted a series of numerical experiments with different subgrid-scale vertical turbulent mixing parametrizations using the WRF model and demonstrated that the vertical turbulent mixing scheme played a significant role in asymmetric structures and eyewall mesovortices of TCs. Smith et al. (2014) examined the sensitivity of TC models to the surface drag coefficient in different PBL schemes and underscored the importance of PBL dynamics in TC intensity forecasting. Tang et al. (2018) investigated the sensitivity of simulated hurricane intensity and structure to two PBL schemes in idealized experiments using the operational Hurricane WRF (HWRF) model.

Recently, Chen and Bryan (2021) performed a set of idealized numerical simulations with the MYNN PBL scheme, and demonstrate that, by adding the advection of TKE, the simulated TC was slightly stronger, and the inner-core size was slightly smaller. Chen et al. (2021b) investigated the effect of the scale-aware Shin–Hong (SH) scheme and non-scale-aware Yonsei University (YSU) scheme on the TC intensification and structural changes and found that the SH scheme tends to produce a stronger TC with a more compact inner core than the YSU scheme. By utilizing a recently developed TC boundary layer modeling framework based on large-eddy simulation (LES, Chen et al., 2021a), Chen (2022) evaluated K-profile parameterization (KPP) schemes as well as high-

order PBL schemes in hurricane conditions. Their results show that different KPP schemes, such as the Global Forecast System (GFS) scheme and the YSU scheme, can result in quite different eddy viscosity K_m and inflow layer, but the performance of both schemes can be improved by adjusting the "shape parameter" of K_m . Wang and Tan (2023) evaluated the uncertainty of the combined effects of cumulus, microphysics, and PBL schemes on TC simulations, and found that the KF cumulus scheme, the Lin microphysics scheme, and the BouLac PBL scheme are the best combination among the evaluated schemes for the TC intensity forecasts.

A key component of a PBL scheme is the parameterization of the vertical turbulent diffusivity of momentum (K_m) and heat (K_h) . Based on the HWRF numerical simulations, researchers have investigated how the turbulent diffusivity of different magnitudes affects the simulated TC intensity and structure (Gopalakrishnan et al., 2013, 2021; Zhang et al., 2015, 2017a, 2017b, 2020). Using idealized HWRF simulations, Gopalakrishnan et al. (2013) show that the magnitudes of K_m and K_h greatly affect the size and intensity changes of simulated TC over the ocean, and reducing K_m to a quarter of its original value produces the best match to the observed MSLP, Zhang et al. (2015, 2017b, 2019) found that the reduction of K_m produced stronger storms with shallower boundary layer, stronger inflow/outflow, and stronger warm core but smaller in storm size. For landfalling TCs, Zhang et al. (2017a) found that vertical turbulent mixing exerted a strong impact on the simulated TC intensity with weaker vertical mixing leading to stronger TC intensity over land. Recently, Zhang et al. (2020) summarized that K_m was an important parameter affecting TC intensity and intensification rate, in particular, a smaller K_m tended to produce a faster storm intensification rate. Using the Hurricane Analysis and Forecast System (HAFS) model, Gopalakrishnan et al. (2021) studied the influence of K_m used in two PBL schemes, a nonlocal K-profile parameterization (KPP) and a TKE scheme, on the TC intensity and structure and found that smaller diffusion leads to larger friction, more vigorous inflow acceleration, and stronger TCs. The above HWRF-based and HAFS-based studies have led to similar conclusions. Besides, based on the nonhydrostatic atmospheric model (NHM) simulation experiments, Kanada et al. (2012) concluded that different values of vertical turbulent diffusivity coefficients result in different TC intensities, inner core structures, and the relationships between maximum wind speed and central pressure. Large vertical eddy diffusivities in lower layers (height < 300 m) lead to large heat and water vapor transfers, resulting in extremely intense TCs accompanied by an upright, contracted eyewall structure. Recently, Xu and Zhao (2021) used the WRF model examined the sensitivity of TC

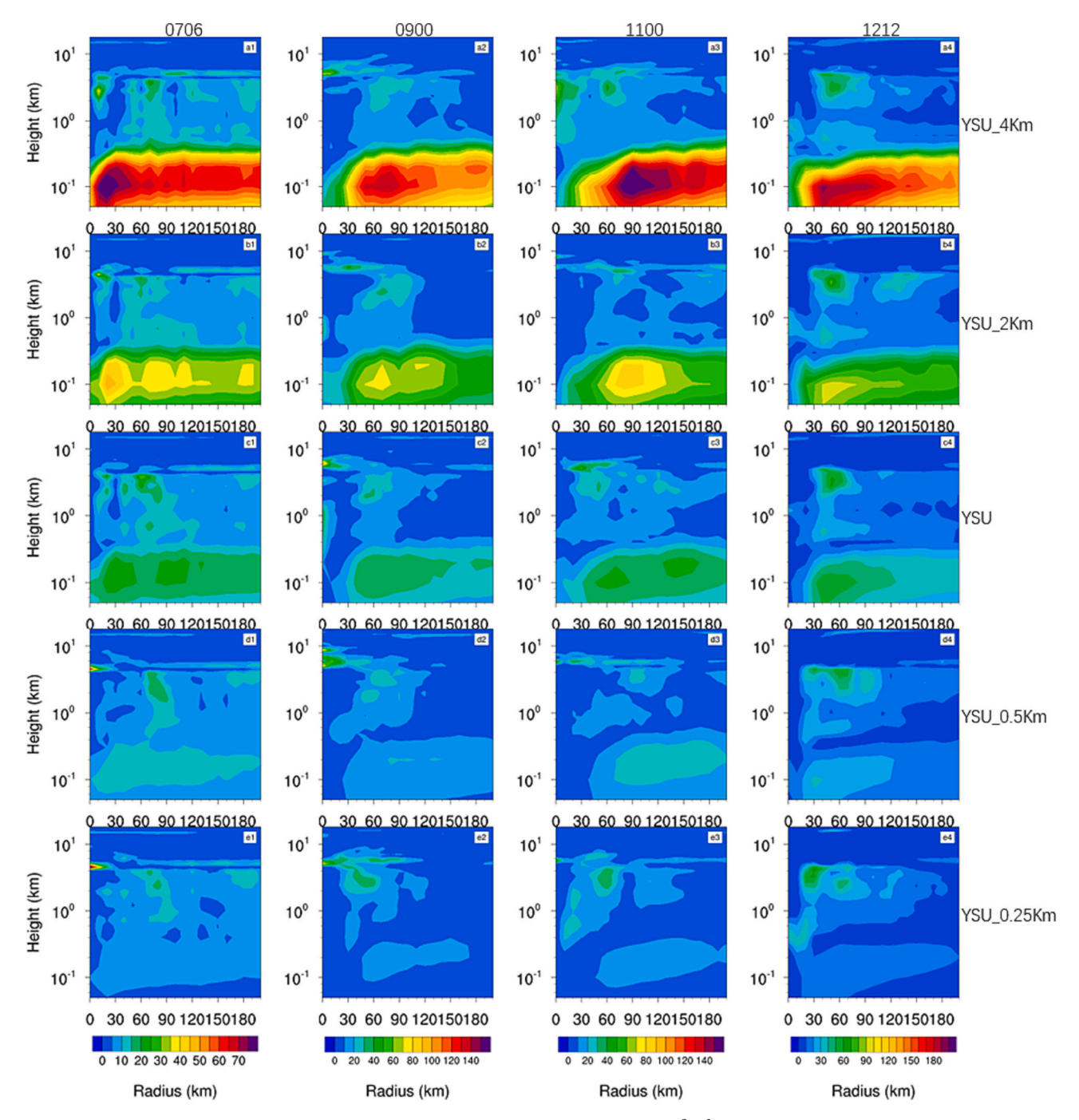


Fig. 2. Height-radius distribution of azimuthally averaged turbulent diffusivity for momentum (unit: $m^2 s^{-1}$) from (a1-a4) YSU_4 K_m , (b1-b4) YSU_2 K_m , (c1-c4) YSU, (d1-d4) YSU_0.25 K_m , and (e1-e4) YSU_0.25 K_m , at (a1-e1) 0600 UTC 7, (a2-e2) 0000 UTC 9, (a3-e3) 0000 UTC 11, and (a4-e4) 1200 UTC 12, September 2018.

simulations to turbulence exchange coefficients for water vapor K_q and momentum K_m and their results showed nonlinear effects of K_q on the simulated TC intensity.

However, previous studies and analyses were basically made based on the grid-point intensity measuring metrics, i.e., examining the minimum central sea level pressure (MSLP) and the maximum 10 m wind speed (VMAX) at model grid points. However, high-resolution numerical studies (e.g., Green and Zhang, 2015; Li et al., 2022) show that the grid-point metrics may not provide a comprehensive evaluation of TC intensity and reveal the underlying dynamics of intensification. Therefore, in this study, using the high-resolution numerical simulations of Typhoon Mangkhut (2018) by the WRF model, we perform a comprehensive evaluation of the sensitivity of TC intensification to the

magnitude of K_m and K_h using two different intensity measuring metrics (i.e., grid-point and area-averaged metrics). For the main purpose of the manuscript, it is to use two intensity metrics (grid-point and area-averaged intensity metrics) to examine the sensitivity of TC intensity simulation to the boundary layer turbulent diffusivity of different magnitude, and to explain the reasons for the different behaviors between K_m to grid-point intensity metrics and K_m to area-averaged intensity metrics from the perspective of TC energy and size. The grid-point intensity metrics are widely used to examine the simulated TC intensity compared to observations, and it is to directly compare with observations. In comparison, the purpose of using the area-averaged intensity metrics is to remove the influence of small-scale processes with randomness and complexities.

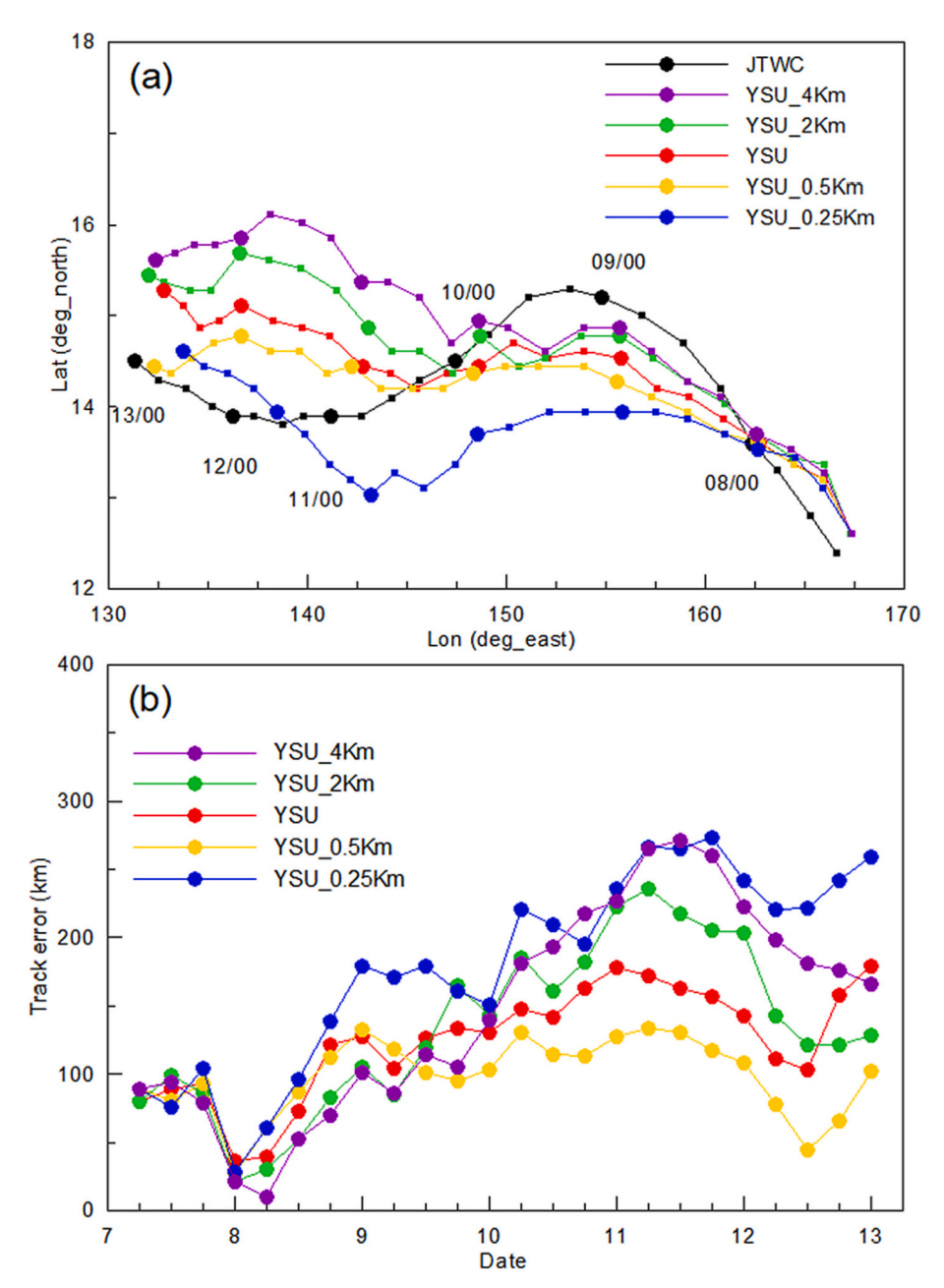


Fig. 3. Comparison of (a) TC track and (b) track error (unit: km) from experiments and JTWC best track data from 0000 UTC 7 to 0000 UTC 13 September 2018.

The rest of the paper is organized as follows. Section 2 introduces Typhoon Mangkhut, the model setup, and the experimental design. Section 3 shows the modification and verification of K_m . Section 4 presents the simulation results and analyses of the underlying. Summary and conclusions are provided in Section 5.

2. Numerical simulations of Typhoon Mangkhut (2018)

2.1. Overview of Typhoon Mangkhut

Mangkhut (2018) formed over the northeastern Pacific and was the 22nd named TC of the 2018 typhoon season (Yang et al., 2019; He et al., 2020b). Its track started from about 2330 km east of Guam on September 7th, then moved westwards and made landfall over Luzon on September 14th (He et al., 2020a; He et al., 2020b). At this time, it reached an estimated maximum sustained wind speed of 250 km h⁻¹. To examine how the turbulent diffusivity K_m and K_h affect the intensification of the

TC, we focus on the intensification period of Mangkhut (2018) from 0000 Universal Time Coordinated (UTC) on September 7th to 0000 UTC on September 13th, 2018. The track and intensity of Mangkhut (2018) during this period can be found in Figs. 1 and 3, respectively.

2.2. Experimental design

The Advanced Research WRF model Version 4.0, developed by the US National Center for Atmospheric Research (NCAR), was utilized in this study. The model was configured with two-way interactive and three-level vortex-following moving nests, as shown in Fig. 1. The outermost to innermost domains consisted of 342×153 , 856×292 , and 433×424 grid points, with horizontal resolutions of 27, 9, and 3 km, respectively. A total of 49 vertical levels were used, with the model top set at 50 hPa. For the initial and lateral boundary conditions, the fifth generation European Center for Medium-Range Weather Forecasts (ECMWF) atmospheric reanalysis of the global climate (ERA5) was

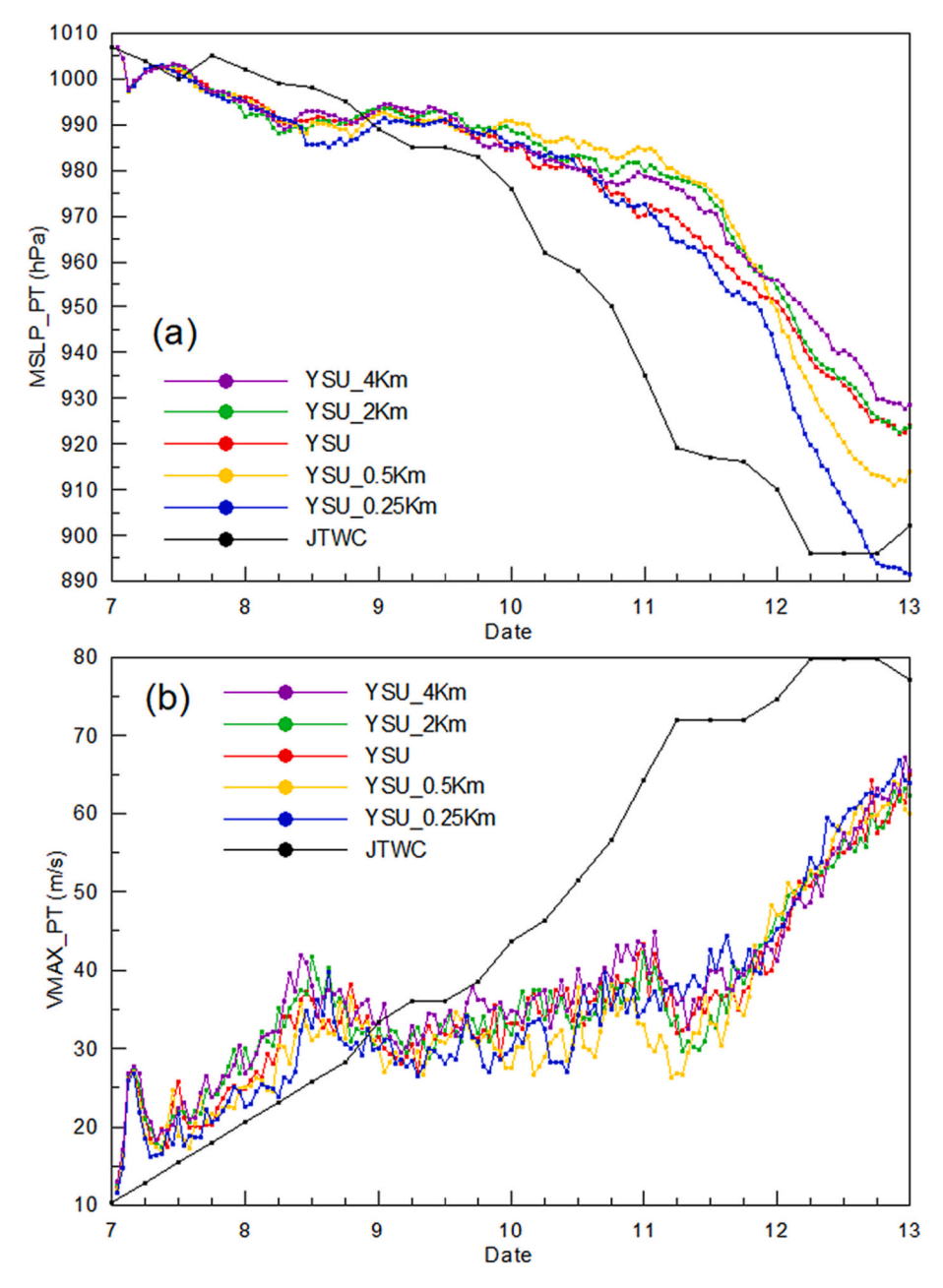


Fig. 4. Time series of point (a) minimum central sea level pressure (MSLP) (unit: hPa) and (b) maximum 10 m wind speed (VMAX) (unit: m s⁻¹).

employed. This dataset has a resolution of $0.25^{\circ} \times 0.25^{\circ}$ and can be accessed at https://cds.climate.copernicus.eu/#!/home. The simulations began at 0000 UTC on September 7th and concluded at 0000 UTC on September 13, 2018, encompassing the intensification period of Typhoon Mangkhut (2018).

The same model physics options were employed for all three domains, with the exception of deactivating the cumulus parameterization in the 9-km and 3-km resolution domains. The physical parameterizations used in this study included the Kain–Fritsch cumulus parameterization scheme (Kain, 2004), the Eta (Ferrier) microphysics scheme (Rogers et al., 2001), the Rapid Radiative Transfer longwave radiation scheme (RRTM) (Mlawer et al., 1997), the Dudhia shortwave radiation scheme (Dudhia, 1989), the Unified Noah land surface model (Tewari et al., 2004), and the Revised MM5 surface layer scheme (Jimenez et al., 2012).

Based on the results from the WRF Physics Use Survey (August 2015) regarding PBL choices (https://www2.mmm.ucar.edu/wrf/users/phys

ics/wrf_physics_survey.pdf), we selected the YSU (Hong et al., 2006) as the PBL scheme for the control experiment in this study. The YSU scheme is widely used and was chosen based on its popularity and established performance in previous research.

3. Modification and verification of K_m

The purpose of a PBL scheme is to parameterize the sub-grid-scale exchanges of moisture, heat, and momentum through mixing, which are associated with turbulent eddies (Cohen et al., 2015). The YSU scheme is a nonlocal and first-order closure scheme that incorporates the explicit entrainment process at the top of the PBL (Hong et al., 2006). In the YSU scheme, for the mixed-layer diffusion, the momentum diffusivity K_m is formulated as

$$K_m = k w_s z \left(1 - \frac{z}{h}\right)^p,\tag{1}$$

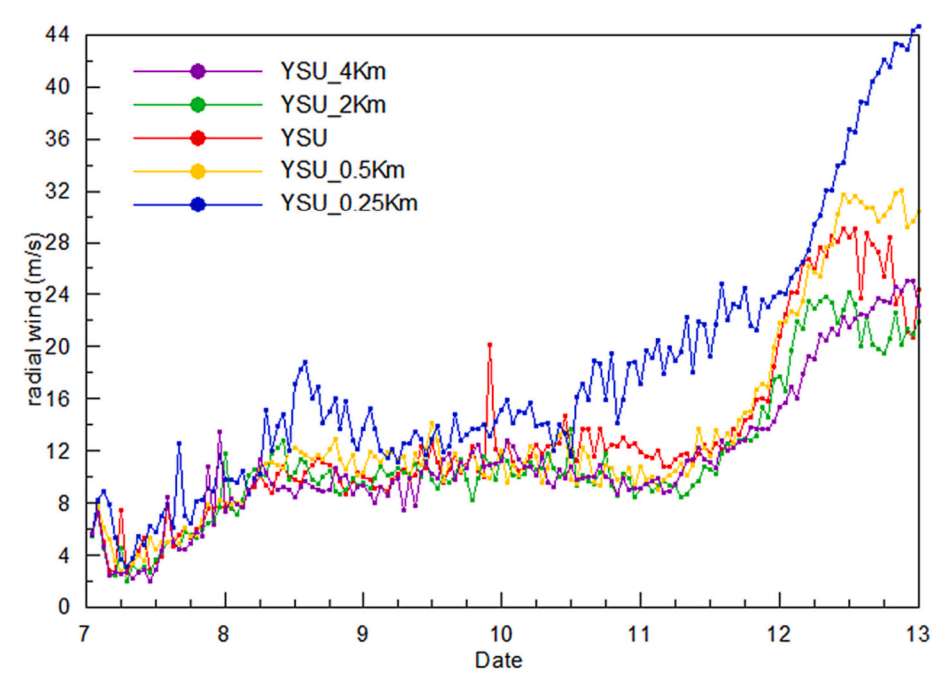


Fig. 5. Time series of maximum azimuthally averaged radial wind speed (unit: m s⁻¹) within 500 km radius and below 1 km height.

where p is the profile shape exponent, taken to be 2, k is the von Kármán constant (≈ 0.4), w_s is the mixed-layer velocity scale, z is the height from the surface, and h is the boundary layer height (or mixed layer height). The diffusivity for heat is parameterized as $K_h = K_m/P_r$, where P_r is Prandtl number.

Chen (2022) concluded that, when compared to the results from LES, the KPP PBL schemes (e.g. YSU and GFS) generally yield less accurate K_m and boundary layer wind profiles compared to the high-order PBL schemes. Additionally, Chen et al. (2021b) pointed out the uncertainty associated with YSU's vertical viscosity and nonlocal transport parameterizations in TC simulations, as they were formulated and validated for the typical continental convective boundary layer. In this study, we conducted a series of sensitivity experiments by modifying the magnitude of K_m in the YSU scheme to investigate the effect of boundary layer turbulent diffusivity on TC simulations.

Following Zhang (2015, 2017), we applied multiplication factors of 4, 2, 0.5, and 0.25 to the turbulent diffusivity for momentum, K_m , in different sensitivity simulation experiments. This approach allowed us to modify the magnitude of K_m and investigate its impact on the simulations. It is worth noting that K_m plays a crucial role as a key parameter in the first-order K-closure PBL schemes. The modification of K_m directly affects the parameterized turbulent fluxes, which in turn provides an opportunity to examine how differently parameterized turbulent fluxes affect the intensification and structural changes of TCs. Table 1 summarizes the modified values of K_m used in different simulation experiments. It is important to note that all experiments share the same model configuration, with the only difference being the magnitude of K_m .

Fig. 2 shows the distribution of K_m simulated by different experiments. Each row represents a different sensitivity experiment, while each column represents a different time point corresponding to different stages of the simulation process. When compared with the original YSU scheme, the sensitivity experiments demonstrate variations in K_m within the boundary layer (approximately below 1 km), with the magnitude increasing or decreasing accordingly to the multiplied coefficient. The results for K_h (figure not shown) follow the same trend as K_m , since K_h is related to K_m through the equation $K_h = K_m/P_r$.

However, single-point metrics can be affected by small-scale processes, such as turbulence and kilometer-scale circulations. These factors can result in high-frequency fluctuations in the local intensity of TCs (e.

g., Rotunno et al., 2009; Xu and Wang, 2021; Li et al., 2022). To remove the impact of these small-scale processes and provide an evaluation of TC intensity at the TC-scale, area-averaged metrics are also introduced in this study. The combination of single-point metrics and area-averaged metrics may provide a more comprehensive evaluation of the effect of K_m on TC intensity simulation.

4. Results

4.1. Point intensity metrics

The simulated tracks are validated using the observed tracks from the Joint Typhoon Warning Center (JTWC) (https://www.metoc.navy.mil/jtwc/jtwc.html). The simulated tracks reproduce the westward movement characteristics of TCs, and their trends are generally consistent with those of the best track data. However, there is still a noticeable deviation between the simulations and observations, particularly during the later hours of the simulation (Fig. 3). Furthermore, Fig. 4 illustrates the point minimum sea level air pressure (MSLP_PT) and point maximum 10 m wind speed (VMAX PT).

The results indicate that during the TC intensification period, the differences among the point MSLPs from the sensitivity experiments are relatively small before 0000 UTC on September 8th and gradually increase starting from about 0000 UTC on September 10th. During the rapid intensification from 1200 UTC on September 10th to 0600 UTC on September 12th, the point MSLPs from the simulations exhibit a nonlinear relationship with the values of K_m . Around 1200 UTC on September 12th, the point MSLP values for all experiments reach their minima. From this time onwards, there is a positive correlation between the point MSLPs and the magnitude of K_m , indicating that smaller K_m produces smaller point MSLP. These findings suggest that during the later stage of intensification (from 0000 UTC on September 12th to 0000 UTC on September 13th), there is a strong correlation between the point MSLPs and the magnitude of K_m . However, this observed agreement between point MSLPs and the magnitude of K_m was not consistently observed before 0000 UTC on September 12th (as shown in Fig. 4) or after 0000 UTC on September 13th (figure not included). This result is consistent with the findings of Gopalakrishnan et al. (2013), who reported that stronger vertical mixing in the PBL during the TC mature

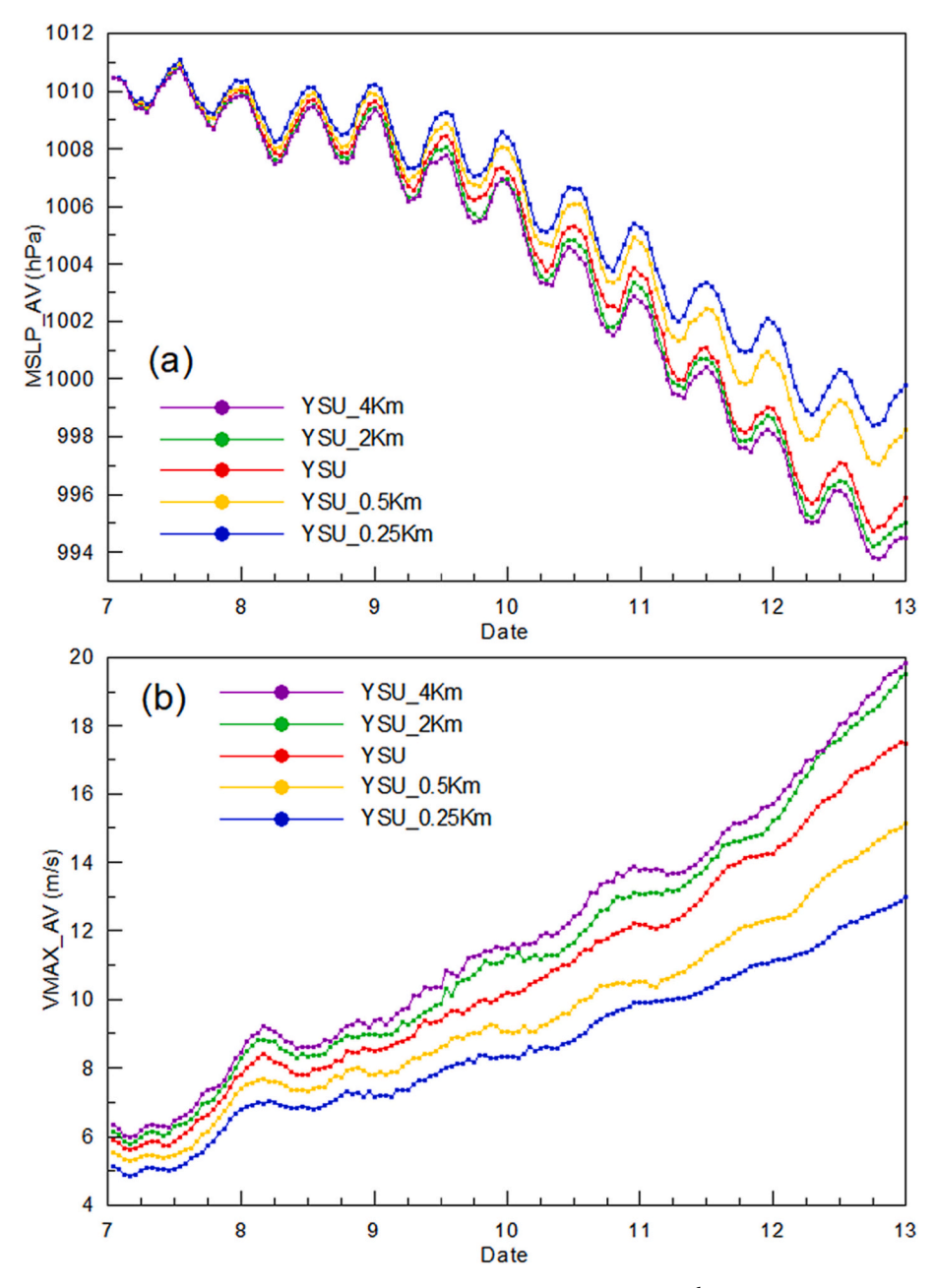


Fig. 6. Time series of area-averaged (a) MSLP (unit: hPa) and (b) VMAX (unit: m s⁻¹) within the radius of 500 km.

stage of a TC leads to a weaker gradient wind imbalance in the eyewall region and favors a larger point MSLP.

Point VMAXs, on the other hand, exhibit significant fluctuations caused by turbulence. Furthermore, the variations of point VMAXs among the different sensitivity experiments do not show a clear correlation with the magnitudes of K_m , except for a weak correlation observed during the intensification period. The point VMAXs from all the experiments converge toward the end of the simulations.

Kepert (2012) demonstrated that large turbulent diffusivity leads to strong mixing, which weaken the surface inflow and eyewall updraft, ultimately reducing storm intensity. This aligns with the conclusion drawn by Gopalakrishnan et al. (2013), Zhang et al. (2015, 2017b), and Xu and Duan (2022) that a small K_m reduces the dissipation of angular momentum in the PBL. As a result, strong radial inflow is promoted, leading to an increase in TC intensity. Our findings are consistent with those of Chen (2022), who illustrated that the YSU scheme with a smaller K_m tends to generate stronger radial inflow at lower levels of the

boundary layer (cf. his Fig. 1). However, the intensity of radial inflow weakens as the "shape parameter" of K_m increases from 2 to 6 (cf. his Fig. 4). Fig. 5 depicts the maximum azimuthally averaged radial inflow simulated by the baseline and sensitivity experiments. Similar to the point MSLP results, the values of the maximum azimuthally averaged radial inflow do not initially appear to correlate with the K_m values during the early simulations. However, as the simulations progress, a clear correlation emerges, whereby smaller K_m values correspond to larger maximum azimuthally averaged radial inflow, consistent with previous studies. Furthermore, the calculated correlation coefficient R between radial wind speed and the magnitude of K_m reveals that in the later stage of simulation, particularly after 0000 UTC on September 12th, the value of correlation coefficient R (-0.63) is significantly smaller than that observed during the early stages of the simulation (ranging from -0.21 to -0.52). This suggests a more pronounced negative correlation between these variables during the later stage of the simulation.

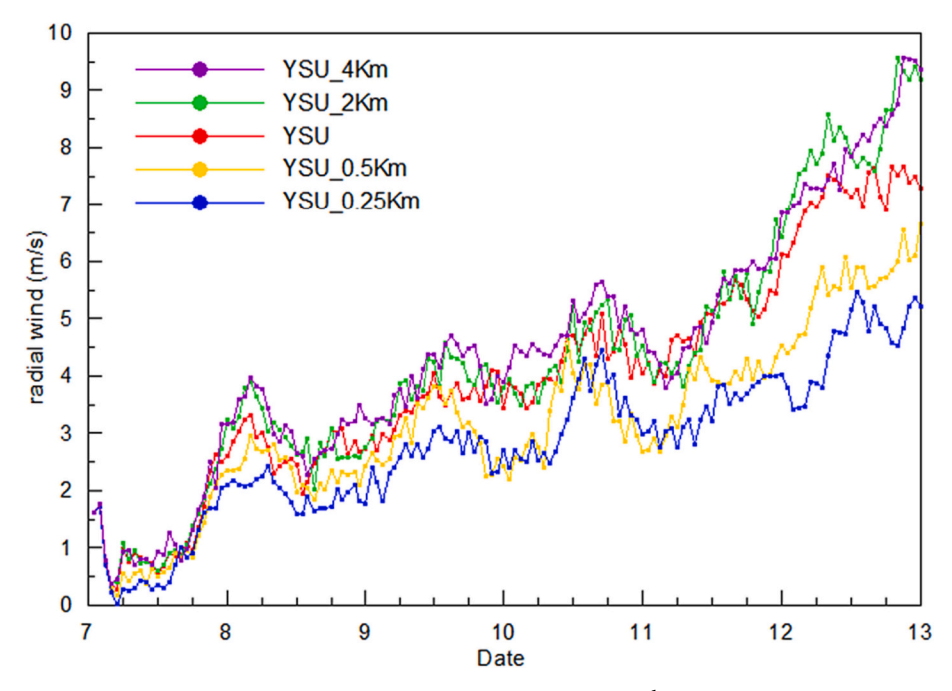


Fig. 7. Time series of area-averaged azimuthally averaged radial wind speed (unit: m s⁻¹) within 500 km radius and below 1 km height.

4.2. Area averaged intensity metrics

As demonstrated in the previous section, the point intensity metrics exhibit a weak relationship between K_m and TC intensity. This suggests that the point intensity metrics are influenced by small-scale processes, such as turbulence eddies and rolls, which introduce randomness and complexities to the variations of the point intensity metrics (Wu et al., 2018; Liu et al., 2021). To remove the influence of these small-scale processes, we adopt area-averaged metrics, following the approach of Rotunno et al. (2009) and Green and Zhang (2015), to examine the relationship among K_m , storm intensity, and radial inflow. Fig. 6 shows the area-averaged MSLP (MSLP AV) and VMAX (VMAX AV) within a 500 km radius, while Fig. 7 depicts the 500 km radius area-averaged radial inflow. A notable observation is that, compared to the point intensity metrics (MSLP_PT and VMAX_PT), the area-averaged metrics (MSLP_AV and VMAX_AV) exhibit a much more consistent relationship between K_m and storm intensity. Specifically, larger values of K_m generally correspond to smaller MSLP_AV and larger VMAX_AV. This finding seems contradictory to the previous observation that larger K_m tends to produce larger MSLP_PT values. Consistent with storm intensity, smaller K_m values result in weaker 500 km radius area-averaged radial inflow. The selection of a 500 km radius is intended to cover areas where wind speeds exceeding 10 m s⁻¹ are prevalent throughout the simulation. By comparing results from an area with a larger radius to those from smaller areas, smoother and more clear linear relationships were observed in the larger radius area. To minimize the influence of smaller areas, we specifically chose a 500 km radius for our analysis. Furthermore, it is worth noting the presence of the semi-diurnal variation in the MSLP_AV field as depicted in Fig. 6(a), whereas it is absent in the MSLP_PT field. To explore and gain a deeper understanding of this phenomenon, further investigation will be necessary in future studies.

4.3. Heat fluxes and diabatic heating

With the variation of K_m in the sensitivity experiments, the surface fluxes, including momentum, sensible heat, and latent heat fluxes are altered. These changes have an impact on convection, as indicated by diabatic heating (Braun and Tao, 2000; Liu et al., 2017; Gopalakrishnan et al., 2013; Ma et al., 2018; Xu and Zhao, 2021). Both the input of heat

fluxes and the release of diabatic heating are significant factors contributing to TC intensification. Therefore, analyzing heat fluxes and diabatic heating serves as a means to understand the connection between K_m variation and TC intensification. This section aims to investigate these variables and provide insights into the reasons for TC intensity variations under different K_m settings.

Fig. 8(a) and (b) present the area-averaged surface sensible and latent heat fluxes within a 500 km radius, respectively. In general, the sensible heat flux accounts for approximately 10% of the latent heat flux, and there are minimal differences among the five simulations. During initial two days of the simulations (from 0000 UTC on September 7th to 0000 UTC on September 9th), when considering that $K_h = K_m/P_r$ as mentioned in Section 3, larger values of K_m generally typically result in larger values of K_h and subsequently higher sensible heat fluxes. This can be attributed to stronger vertical mixing. However, beyond this period, the variations in sensible heat flux among the five simulations become negligible (except for YSU_0.25K_m, which is considerably smaller than the others toward the end of the simulation). Fig. 8 illustrates that the sensible heat fluxes of the simulations with larger K_m values, such as $YSU_{-}4K_{m}$, $YSU_{-}2K_{m}$, and YSU, are greater compared to those with YSU_0.5K_m and YSU_0.25K_m. The stronger surface winds associated with larger K_m values would also contribute to increased sensible heat fluxes. Nevertheless, due to greater fluctuations and smaller magnitude orders of the sensible heat flux, Fig. 8(a) reveals no apparent linear relationship between the sensible heat flux and K_m , unlike the latent heat flux and K_m . This is likely influenced by a negative feedback mechanism between the sensible heat flux and K_m , since larger K_m values tend to generate a warmer PBL, thereby reducing the air-sea thermal contrast. Conversely, the latent heat flux exhibits a nearly linear relationship with the magnitude of K_m throughout the simulations. This can be attributed to the fact that larger K_m values promote stronger ventilation in the surface layer, leading to enhanced surface evaporation.

Fig. 9 compares the sum of diabatic heating energy within a radius of 500 km from the TC center among different experiments. The results show that a larger K_m generates greater storm-scale diabatic heating. However, the relationship between K_m and diabatic heating is not as linear as the relationship between latent heat flux shown in Fig. 8(b). This non-linearity is partly caused by spontaneous convection, and

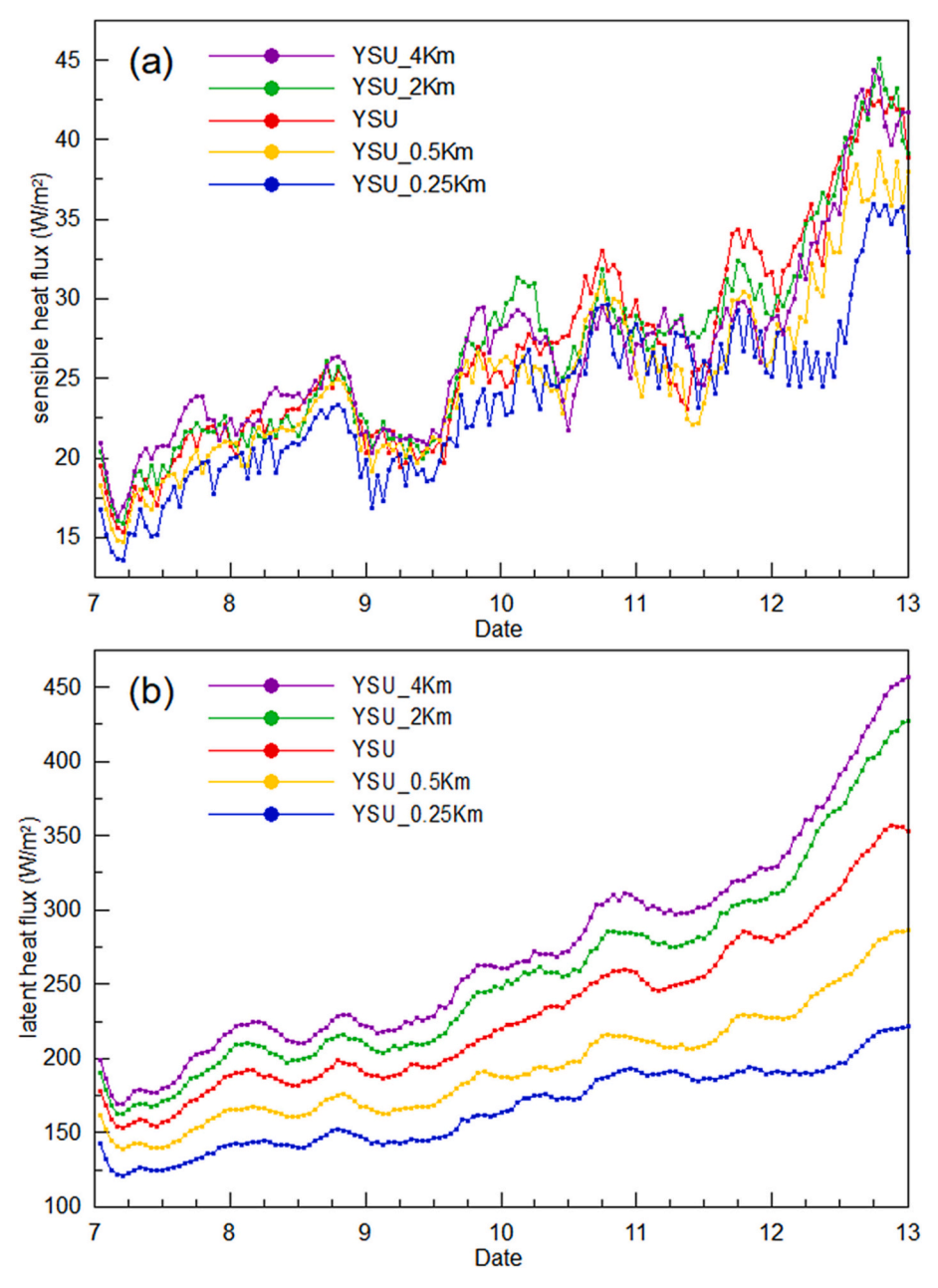


Fig. 8. Time series of area-averaged surface (a) sensible heat flux (unit: $W m^{-2}$) and (b) latent heat flux (unit: $W m^{-2}$) within the radius of 500 km.

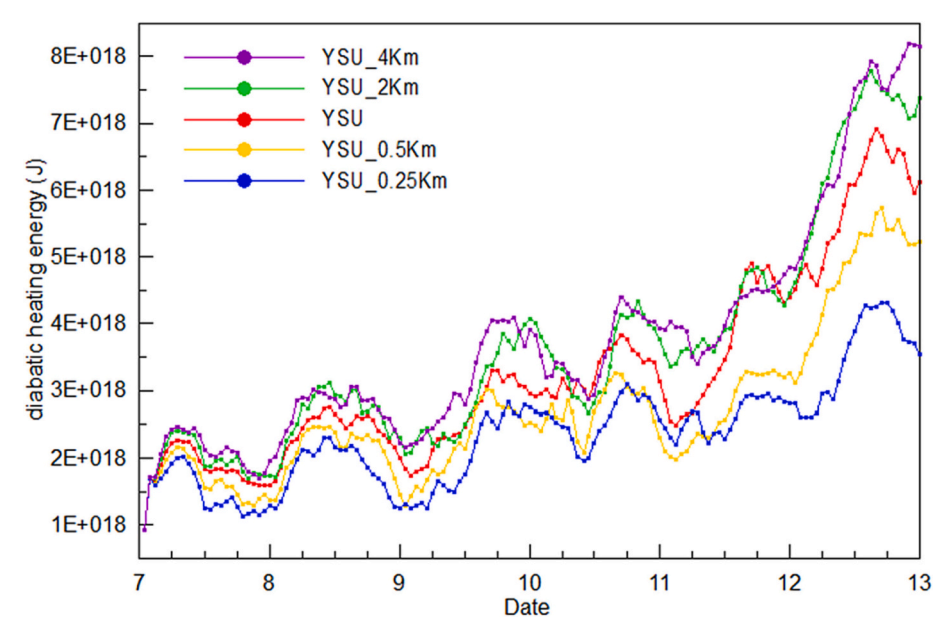


Fig. 9. Time series of area sum of diabatic heating energy (unit: J) within the radius of 500 km and below the height of 15 km.

partly caused by the complex dynamics of a TC. Our results are consistent with the fact that larger diabatic heating can lead to an increase in air temperature, hindering the air parcel from reaching saturation, and therefore inhibiting the further release of diabatic heating. The findings in Fig. 9 are consistent with previous studies by Zhu et al. (2014) and Zhang et al., (Zhang et al., 2015; Zhang et al., 2017b), who concluded that larger vertical mixing transports more heat from the ocean surface upwards to foster atmospheric convection. However, we note that the larger area-mean diabatic heating does not necessarily guarantee stronger individual connective cells, as it is more affected by the size of a TC, which will be discussed in the next section.

4.4. TC size

TC size is commonly defined using the radius of the 10 m tangential wind (ut10) with a specified speed (Schenkel et al., 2017; Bian et al., 2021). Following Schenkel et al. (2017) and Bian et al. (2021), we used the radius of ut10 of 10 m s $^{-1}$ (R10) to define the size of TCs simulated in this study.

Fig. 10(a)-(e) show the time-radius variations of the azimuthally averaged ut10 in the five simulations. The larger K_m generally tends to produce larger ut10, consistent with the findings in Section 4.2. Fig. 11 further compares the time variation of R10 among the experiments. It again shows a nearly linear relationship between K_m and R10, with a larger K_m corresponding to a larger R10. Since a larger R10 means the expansion of a TC, such an expansion should exert a negative impact on the point MSLP (i.e., increases the point MSLP). If the pressure gradient force for the 10 m wind remains constant, a larger R10 would result in a greater distance from the TC center. Consequently, the pressure at the TC center would be higher, given the same pressure gradient force. This explains why the K_m -intensity relationship shows contradictory results between the grid-point metrics and the area-averaged metrics. This result is consistent with Zhang et al. (2020), although they used the radius of maximum wind (RMW) as the TC size indicator.

Regarding the relationship of TC intensity and K_m , on the one hand, a smaller K_m produces a larger grid-point intensity. On the other hand, a larger K_m produces a larger area-averaged intensity. For this contradictory relationship, compared with a single grid point, with the expansion of the area and the increase of TC size, a larger K_m produces stronger latent heat flux and diabatic heat energy from the area, which leads to the generation of stronger TC storms.

5. Summary and conclusions

Motivated by previous studies on the effect of turbulent diffusivity K_m on TC simulations, this study revisits the problem using a set of sensitivity experiments performed by the WRF model with modified K_m of the YSU scheme. Two different methods, namely, the grid-point and area-averaged intensity metrics, are used to evaluate the simulations. The main findings are summarized as follows.

In the evaluation using grid-point intensity metrics, it is found that grid-point MSLPs are well correlated with the magnitudes of K_m , with a smaller K_m producing a smaller point MSLP. However, due to fluctuations caused by the asymmetric eddy features, grid-point VMAXs are only weakly correlated to K_m . Zhu et al. (2019, 2021) pointed out that the asymmetric eddy processes provide an important forcing for the evolution of the primary circulation of a TC. Similar to grid-point MSLP, the maximum azimuthally averaged radial inflow in these experiments correlates well with the magnitude of K_m , with a smaller K_m corresponding to a larger maximum azimuthally averaged radial inflow. These findings are consistent with previous studies (e.g., Gopalakrishnan et al., 2013; Zhang et al., 2015, 2017b) that have shown the reduction of K_m enhances radial inflow, leading to stronger TC intensity for a mature TC.

Unlike the grid-point intensity metrics, the area-averaged MSLP and VMAX show a much more consistent relationship with K_m . A larger K_m tends to produce a smaller MSLP_AV and a larger VMAX_AV, which is consistent with a stronger 500 km radius area-averaged radial inflow throughout the simulations.

The comparison of surface heat fluxes reveals that the sensible heat flux accounts for approximately 10% of the latent heat flux, and the differences in sensible heat flux among the simulations are minimal. On the other hand, the latent heat flux shows a nearly linear relationship with K_m throughout the simulations. Nevertheless, due to the spontaneous asymmetric convective eddy features, the relationship between K_m and diabatic heating is not as clean as that between K_m and latent heat flux. Overall, a larger K_m tends to generate greater diabatic heating, leading to stronger TC intensity, which is consistent with the findings of Zhang et al. (2017b).

Using R10 as the size indicator of a TC, the results indicate that a larger K_m tends to result in a larger ut10, which is consistent with previous findings. Additionally, R10 shows a clear linear relationship with K_m throughout the simulations, with a larger K_m corresponding to a

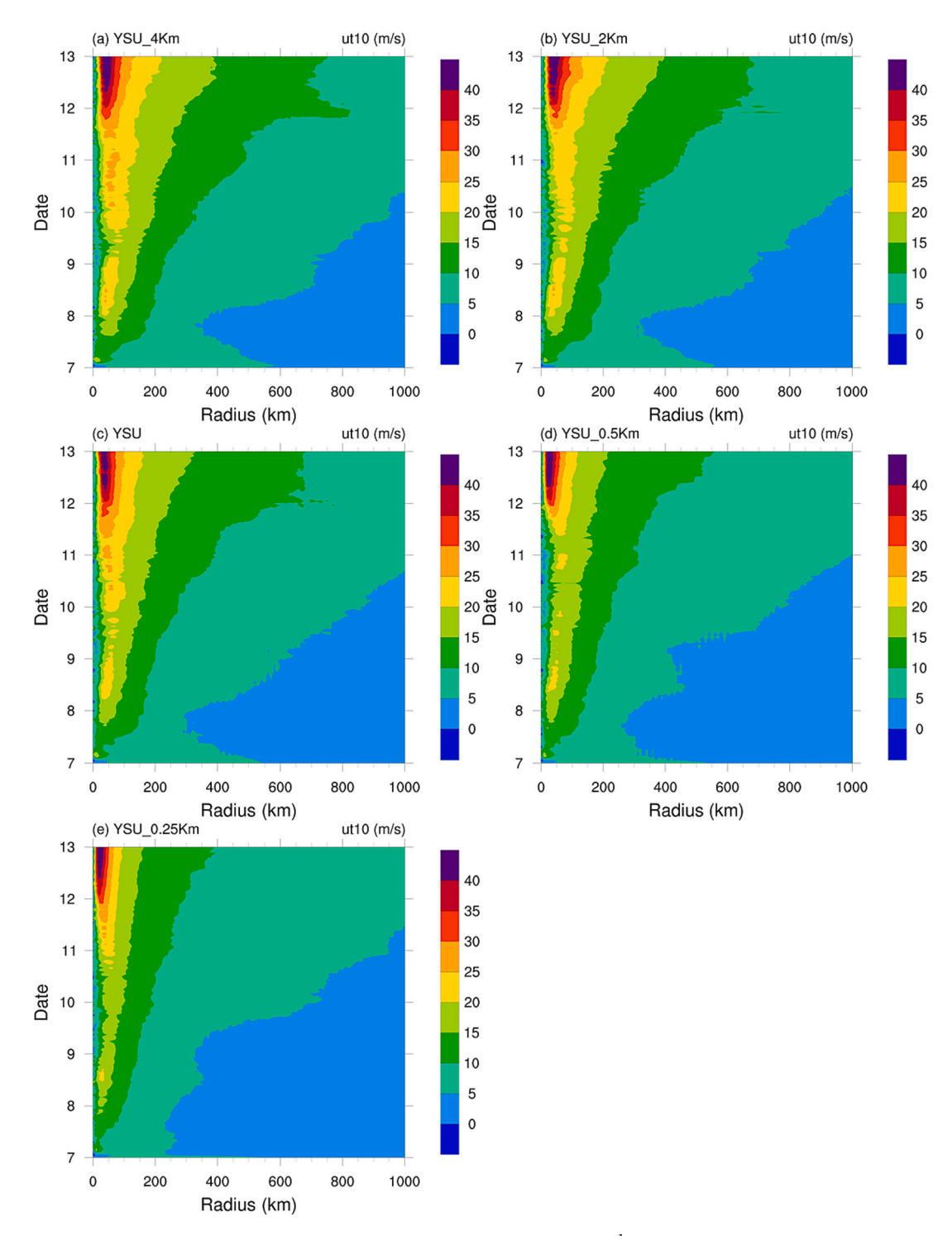


Fig. 10. Hovmoller diagram of azimuthally averaged 10 m tangential wind speed (unit: m s^{-1}) in (a) YSU_4 K_m , (b) YSU_2 K_m , (c) YSU, (d) YSU_0.5 K_m , (e) YSU_0.25 K_m .

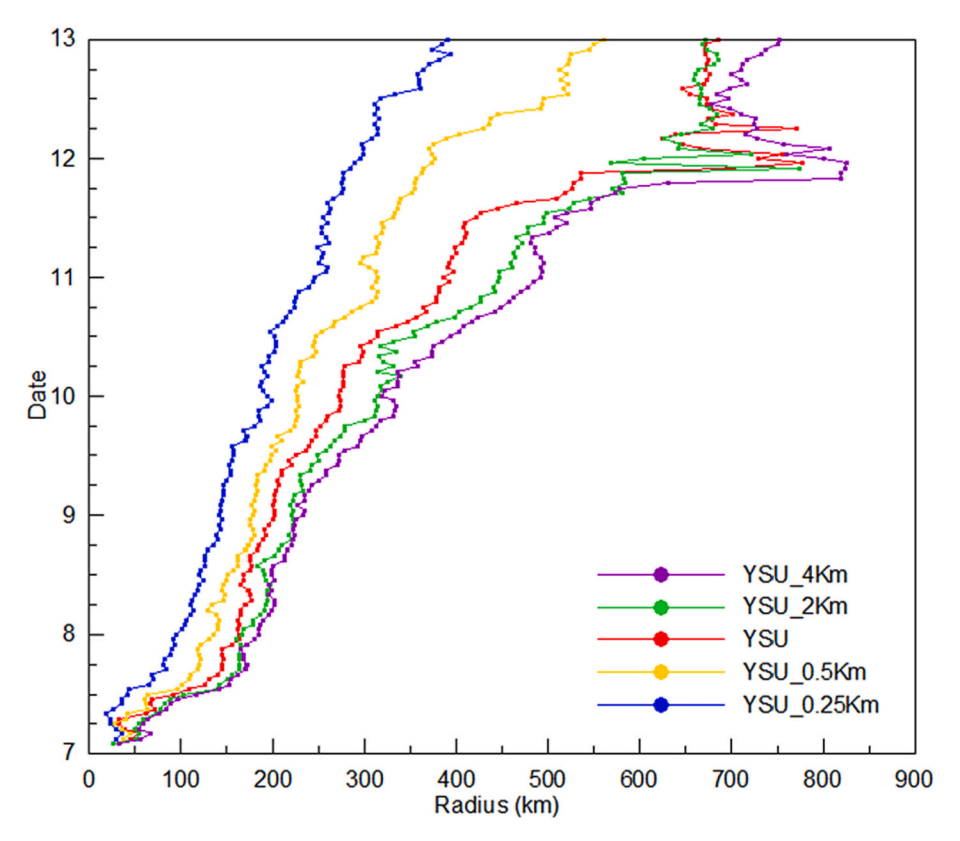


Fig. 11. Time series of R10 (radius of 10 m tangential wind speed at 10 m s⁻¹, unit: km).

larger R10. Since a larger R10 represents the expansion of a TC, such expansion would have a negative impact (i.e., increase) on the grid-point MSLP. This explains why the grid-point K_m -intensity metrics exhibit a contradictory relationship compared to the area-averaged metrics. The findings of this study highlight the need for research efforts are aimed at providing physical constraints on turbulent diffusivities for TC simulations using observations.

CRediT authorship contribution statement

Lei Ye: Methodology, Software, Validation, Formal analysis, Investigation, Data curation, Writing – original draft, Visualization. Yubin Li: Conceptualization, Formal analysis, Writing – review & editing, Project administration, Funding acquisition. Ping Zhu: Formal analysis, Writing – review & editing. Zhiqiu Gao: Writing – review & editing, Supervision, Project administration.

Declaration of Competing Interest

The authors declare that they have no known competing financial interests or personal relationships that could have appeared to influence the work reported in this paper.

Data availability

I have shared the link to the data used

Acknowledgements

This study is supported by the National Natural Science Foundation of China (42075072), Ping Zhu acknowledges his support by NSF under the grant number 2211307 and by NOAA under the grant number NA22OAR4590177. The numerical calculations in this paper have been

done on the supercomputing system in the Supercomputing Center of Nanjing University of Information Science & Technology.

References

Bian, G.F., Nie, G.Z., Qiu, X., 2021. How well is outer tropical cyclone size represented in the ERA5 reanalysis dataset? Atmos. Res. 249, 105339.

Braun, S.A., Tao, W.K., 2000. Sensitivity of high-resolution simulations of Hurricane Bob (1991) to planetary boundary layer parameterizations. Mon. Weather Rev. 128, 3941–3961

Chang, Y., Yang, S., Lin, K., Lien, G., Wu, C., 2020. Impact of tropical cyclone initialization on its convection development and intensity: a case study of Typhoon Megi (2010). J. Atmos. Sci. 77 (2), 443–464.

Charney, J.G., Eliassen, A., 1964. On the growth of the hurricane depression. J. Atmos. Sci. 21, 68–75.

Chen, X., 2022. How do planetary boundary layer schemes perform in hurricane conditions: a comparison with large-eddy simulations. J. Adv. Model. Earth Syst. 14, e2022MS003088.

Chen, X., Bryan, G.H., 2021. Role of advection of parameterized turbulence kinetic energy in idealized tropical cyclone simulations. J. Atmos. Sci. 78 (11), 3559–3574.
 Chen, X., Bryan, G.H., Zhang, J.A., Cione, J.J., Marks, F.D., 2021a. A framework for simulating the tropical-cyclone boundary layer using large-eddy simulation and its

use in evaluating PBL parameterizations. J. Atmos. Sci. 78 (11), 3593–3611. Chen, X., Xue, M., Zhou, B., Fang, J., Zhang, J.A., Marks, F.D., 2021b. Effect of scale-aware planetary boundary layer schemes on tropical cyclone intensification and structural changes in the gray zone. Mon. Weather Rev. 149 (7), 2079–2095.

Cohen, A.E., Cavallo, S.M., Coniglio, M.C., Brooks, H., 2015. A review of planetary boundary layer parameterization schemes and their sensitivity in simulating a Southeast U.S. cold season severe weather environment. Weather Forecast. 30, 501–612.

Dudhia, J., 1989. Numerical study of convection observed during the Winter Monsoon Experiment using a mesoscale two-dimensional model. J. Atmos. Sci. 46, 2027, 2107

Emanuel, K.A., 2003. Tropical cyclone. Annu. Rev. Earth Planet. Sci. 31, 75–104.
Emanuel, K.A., 2018. 100 years of progress in tropical cyclone research. Meteorol.
Monogr. 59, 15.1–15.68.

Fox, K.R., Judt, F., 2018. A numerical study on the extreme intensification of hurricane patricia (2015). Weather Forecast. 33 (4), 989–999.

Gopalakrishnan, S.G., Marks, F., Zhang, J.A., Zhang, X., Bao, J.W., Tallapragada, V., 2013. A study of the impacts of vertical diffusion on the structure and intensity of the tropical cyclones using the high-resolution HWRF system. J. Atmos. Sci. 70, 524–541.

- Gopalakrishnan, S.G., Hazelton, A., Zhang, J.A., 2021. Improving hurricane boundary layer parameterization scheme based on observations. Earth Space Sci. 8, e2020EA001422.
- Green, B.W., Zhang, F., 2015. Numerical simulations of Hurricane Katrina (2005) in the turbulent gray zone. J. Adv. Model Earth Syst. 7 (1), 142–161.
- He, Q., Zhang, K., Wu, S., Zhao, Q., Wang, X., Shen, Z., Li, L., Wan, M., Liu, X., 2020a. Real-time GNSS-derived PWV for Typhoon characterizations: a case study for super Typhoon Mangkhut in Hong Kong. Remote Sens. 12, 104.
- He, Y.C., He, J.Y., Chen, W.C., Chan, P.W., Fu, J.Y., Li, Q., 2020b. Insights from super Typhoon Mangkhut (1822) for wind engineering practices. J. Wind Eng. Ind. Aerodyn. 203, 104238.
- Hong, S.Y., Noh, Y., Dudhia, J., 2006. A new vertical diffusion package with an explicit treatment of entrainment processes. Mon. Weather Rev. 134, 2318–2341.
- Jimenez, P.A., Dudhia, J., Gonzalez-Rouco, J.F., Navarro, J., Montavez, J.P., Garcia-Bustamante, E., 2012. A revised scheme for the WRF surface layer formulation. Mon. Weather Rev. 140, 898–918.
- Kain, J.S., 2004. The Kain–Fritsch convective parameterization: an update. J. Appl. Meteorol. 43, 170–181.
- Kanada, S., Wada, A., Nakano, M., Kato, T., 2012. Effect of planetary boundary layer schemes on the development of intense tropical cyclones using a cloud-resolving model. J. Geophys. Res. 117, D03107.
- Kaplan, J., Rozoff, C.M., DeMaria, M., Sampson, C.R., Kossin, J.P., Velden, C.S., Cione, J. J., Dunion, J.P., Knaff, J.A., Zhang, J.A., Dostalek, J.F., Hawkins, J.D., Lee, T.F., Solbrig, J.E., 2015. Evaluating environmental impacts on tropical cyclone rapid intensification predictability utilizing statistical models. Weather Forecast. 30, 1374–1396
- Kepert, J.D., 2012. Choosing a Boundary Layer Parameterization for Tropical Cyclone Modeling. Mon. Weather Rev. 140 (5), 1427–1445.
- Lee, J., Wu, C., 2018. The role of polygonal eyewalls in rapid intensification of Typhoon Megi (2010). J. Atmos. Sci. 75 (12), 4175–4199.
- Li, X., Pu, Z., 2008. Sensitivity of numerical simulation of early rapid intensification of hurricane Emily (2005) to cloud microphysical and planetary boundary layer parameterizations. Mon. Weather Rev. 136, 4819–4838.
- Li, T.H., Wang, Y., 2021a. The role of boundary layer dynamics in tropical cyclone intensification. Part I: Sensitivity to surface drag coefficient. J. Meteorol. Soc. Jpn. 99, 537–554.
- Li, T.H., Wang, Y., 2021b. The role of boundary layer dynamics in tropical cyclone intensification. Part II: Sensitivity to initial vortex structure. J. Meteorol. Soc. Jpn. 99, 555–573.
- Li, Y., Zhu, P., Gao, Z., Cheung, K.K., 2022. Sensitivity of large eddy simulations of tropical cyclone to sub-grid scale mixing parameterization. Atoms. Res. 265, 105922.
- Liu, J., Zhang, F., Pu, Z., 2017. Numerical simulations of the rapid intensification of Hurricane Katrina (2005): Sensitivity to boundary layer parameterization schemes. Adv. Atmos. Sci. 34 (4), 482–496.
- Liu, Q., Wu, L., Qin, N., Li, Y., 2021. Storm-scale and fine-scale boundary layer structures of tropical cyclones simulated with the WRF-LES framework. J. Geophys. Res. Atmos. 126, e2021 ID035511
- Ma, Z., Fei, J., Huang, X., Cheng, X., 2018. Sensitivity of the simulated tropical cyclone intensification to the boundary-layer height based on a K-profile boundary-layer parameterization scheme. J. Adv. Model Earth Syst. 10, 2912–2932.
- Ming, J., Zhang, J.A., 2018. Direct measurements of momentum flux and dissipative heating in the surface layer of tropical cyclones during landfalls. J. Geophys. Res. 123 (10), 4926–4938.
- Mlawer, E.J., Taubman, S.J., Brown, P.D., Iacono, M.J., Clough, S.A., 1997. Radiative transfer for inhomogeneous atmospheres: RRTM, a validated correlated-k model for the longwave. J. Geophys. Res. 102, 16663–16682.
- Montgomery, M.T., Smith, R.K., 2014. Paradigms for tropical cyclone intensification. Aust. Meteorol. Ocean. J. 64, 37–66.
- Nystrom, R.G., Chen, X., Zhang, F., Davis, C.A., 2020. Nonlinear impacts of surface exchange coefficient uncertainty on tropical cyclone intensity and air–sea interactions. Geophys. Res. Lett. 47, e2019GL085783.
- Ooyama, K.V., 1964. A dynamical model for the study of tropical cyclone development. Geofis. Int. 4, 187–198.
- Ooyama, K.V., 1982. Conceptual evolution of the theory and modeling of the tropical cyclone. J. Meteorol. Soc. Jpn. 60, 369–380.
- Rogers, E., Black, T., Ferrier, B., Lin, Y., Parrish, D., DiMego, G., 2001. Changes to the NCEP Meso Eta Analysis and Forecast System: Increase in Resolution, New Cloud

- Microphysics, Modified Precipitation Assimilation, and Modified 3DVAR Analysis. NWS Tech. Procedures Bull. 488, NOAA/NWS.
- Rotunno, R., Chen, Y., Wang, W., Davis, C., Dudhia, J., Holland, G.J., 2009. Large-eddy simulation of an idealized tropical cyclone. Bull. Am. Meteorol. Soc. 90 (12), 1783–1788.
- Schenkel, B.A., Lin, N., Chavas, D., Oppenheimer, M., Brammer, A., 2017. Evaluating outer tropical cyclone size in reanalysis datasets using QuikSCAT data. J. Clim. 30, 8745–8762.
- Smith, R.K., Montgomery, M.T., Thomsen, G.L., 2014. Sensitivity of tropical-cyclone models to the surface drag coefficient in different boundary-layer schemes. Q. J. R. Meteorol. Soc. 140 (680), 792–804.
- Sun, X., Barros, A.P., 2014. High resolution simulation of tropical storm Ivan (2004) in the Southern Appalachians: role of planetary boundary-layer schemes and cumulus parametrization. Q. J. R. Meteorol. Soc. 140, 1847–1865.
- Sun, J., He, H., Hu, X., Wang, D., Gao, C., Song, J., 2019. Numerical simulations of Typhoon Hagupit (2008) using WRF. Weather Forecast. 34 (4), 999–1015.
- Tang, J., Zhang, J.A., Kieu, C., Marks, F.D., 2018. Sensitivity of hurricane intensity and structure to two types of planetary boundary layer parameterization schemes in idealized HWRF simulations. Trop. Cyclone Res. Rev. 7 (4), 201–211.
- Tewari, M., Chen, F., Wang, W., Dudhia, J., LeMone, M.A., Mitchell, K., Ek, M., Gayno, G., Wegiel, J., Cuenca, R.H., 2004. Implementation and verification of the unified NOAH land surface model in the WRF model. In: 20th Conference on Weather Analysis and Forecasting/16th Conference on Numerical Weather Prediction, pp. 11–15.
- Wang, X., Tan, Z., 2023. On the combination of physical parameterization schemes for tropical cyclone track and intensity forecasts in the context of uncertainty. J. Adv. Model. Earth Syst. 15, e2022MS003381.
- Wang, H., Wang, Y., 2014. A numerical study of Typhoon Megi (2010). Part I: Rapid intensification. Mon. Weather Rev. 142 (1), 29–48.
- Wu, L., Liu, Q., Li, Y., 2018. Prevalence of tornado-scale vortices in the tropical cyclone eyewall. Proc. National Academy Sci. 115 (33), 8307–8310.
- Xu, H., Duan, Y., 2022. Sensitivity of the tropical cyclone boundary layer to vertical diffusion in a turbulent kinetic energy-based boundary layer parameterization scheme at gray-zone resolution. J. Geophys. Res. Atmos. 127, e2021JD035601.
- Xu, H., Wang, Y., 2021. Sensitivity of fine-scale structure in tropical cyclone boundary layer to model horizontal resolution at sub-kilometer grid spacing. Front. Earth Sci. 9, 707274.
- Xu, H., Zhao, D., 2021. Effect of the vertical diffusion of moisture in the planetary boundary layer on an idealized tropical cyclone. Adv. Atmos. Sci. 38 (11), 1889–1904.
- Yang, J., Li, L., Zhao, K., Wang, P., Wang, D., Sou, I.M., Yang, Z., Hu, J., Tang, X., Mok, K. M., Liu, P.L.F., 2019. A comparative study of Typhoon Hato (2017) and Typhoon Mangkhut (2018) their impacts on coastal inundation in Macau. J. Geophys. Res. Oceans. 124, 9590–9619.
- Zhang, J.A., Rogers, R.F., 2019. Effects of parameterized boundary layer structure on hurricane rapid intensification in shear. Mon. Weather Rev. 147 (3), 853–871.
- Zhang, J.A., Nolan, D.S., Rogers, R.F., Tallapragada, V., 2015. Evaluating the impact of improvements in the boundary layer parameterization on hurricane intensity and structure forecasts in HWRF. Mon. Weather Rev. 143, 3136–3155.
- Zhang, F., Pu, Z., Wang, C., 2017a. Effects of boundary layer vertical mixing on the evolution of hurricanes over land. Mon. Weather Rev. 145 (6), 2343–2361.
- Zhang, J.A., Rogers, R.F., Tallapragada, V., 2017b. Impact of parameterized boundary layer structure on tropical cyclone rapid intensification forecasts in HWRF. Mon. Weather Rev. 145 (4), 1413–1426.
- Zhang, J.A., Kalina, E.A., Biswas, M.K., Rogers, R.F., Zhu, P., Marks, F.D., 2020. A review and evaluation of planetary boundary layer parameterizations in Hurricane weather research and forecasting model using idealized simulations and observations. Atmosphere. 11, 1091.
- Zhu, P., Menelaou, K., Zhu, Z., 2014. Impact of subgrid-scale vertical turbulent mixing on eyewall asymmetric structures and mesovortices of hurricanes. Q. J. R. Meteorol. Soc. 140 (679), 416–438.
- Zhu, P., Tyner, B., Zhang, J.A., Aligo, E., Gopalakrishnan, S., Marks, F.D., Mehra, A., Tallapragada, V., 2019. Role of eyewall and rainband eddy forcing in tropical cyclone intensification. Atmos. Chem. Phys. 19 (22), 14289–14310.
- Zhu, P., Hazelton, A., Zhang, Z., Marks, F.D., Tallapragada, V., 2021. The role of eyewall turbulent transport in the pathway to intensification of tropical cyclones. J. Geophys. Res. Atmos. 126, e2021JD034983.